DALTON
FULL PAPER

Mercury(II), silver(I) and gold(I) thioether crown chemistry: synthesis, electrochemistry and structures of $[(HgBr_2)_2([24]aneS_8)]$, $[\{Ag_2([24]aneS_8)(CF_3SO_3)_2(MeCN)_2\}_\infty]$, $[Ag_2([28]aneS_8)][NO_3]_2$ and $[Au_2([28]aneS_8)][PF_6]_2$ ([24]aneS$_8$ = 1,4,7,10,13,16,19,22-octathiacyclotetracosane; [28]aneS$_8$ = 1,4,8,11,15,18,22,25-octathiacyclooctacosane)

Alexander J. Blake, Wan-Sheung Li, Vito Lippolis, Anne Taylor and Martin Schröder *

Department of Chemistry, The University of Nottingham, Nottingham, UK NG7 2RD

The complexes $[(HgBr_2)_2([24]aneS_8)]$, $[\{Ag_2([24]aneS_8)(CF_3SO_3)_2(MeCN)_2\}_\infty]$ ([24]aneS$_8$ = 1,4,7,10,13,16,19,22-octathiacyclotetracosane), $[Au_2([28]aneS_8)][PF_6]_2$ and $[Ag_2([28]aneS_8)][NO_3]_2$ ([28]aneS$_8$ = 1,4,8,11,15,18,22,25-octathiacyclooctacosane) have been synthesized, characterised and their crystal structures determined. In $[(HgBr_2)_2([24]aneS_8)]$ two $HgBr_2$ units are bound to the macrocycle forming a discrete binuclear complex, Hg(1)–Br(1) 2.511(2), Hg(1)–Br(2) 2.588(2), Hg(1)–S(4) 2.835(4), Hg(1)–S(7) 2.581(4) Å. In $[\{Ag_2([24]aneS_8)(CF_3SO_3)_2(MeCN)_2\}_\infty]$ infinite polymeric chains of [24]aneS$_8$ molecules and silver(I) ions are observed, Ag(1)–S(1) 2.5400(14), Ag(1)–S(4) 2.627(2), Ag(1)–S(7^i) 2.556(2), Ag(1)–S(10^i) = 2.5984(14) Å (i x, $y + 1$, z), with the large-ring crown acting as a bidentate ligand to two tetrahedral silver(I) centres. In contrast, $[Ag_2([28]aneS_8)][NO_3]_2$ is a binuclear complex with each Ag^I co-ordinated to four S-donors of the macrocyclic ligand, Ag(1)–S(1) 2.5257(12), Ag(1)–S(4) 2.6314(11), Ag(1)–S(8) 2.8932(12), Ag(1)–S(11) 2.4921(11) Å, and one NO_3^- completing a very distorted trigonal bipyramidal co-ordination sphere, Ag(1)–O(2) 2.759(3) Å. In $[Au_2([28]aneS_8)][PF_6]_2$ two gold(I) centres are complexed tetrahedrally within the octathiamacrocycle in a [2 + 2] manner, Au(1)–S(1) 2.330(2), Au(1)–S(4) 2.789(2), Au(1)–S(8) 2.763(2), Au(1)–S(11) 2.338(2) Å. The redox properties of the complexes are described.

In recent years the co-ordination chemistry of crown thioethers has attracted much attention.[1] These macrocycles show a remarkable ability to form stable and inert complexes with a wide range of d-[2–12] and p-block[13] elements, in many cases forcing the metal centre to adopt unusual co-ordination geometries or oxidation states.[1,14,15] The thioethers employed in these studies have principally been 1,4,7-trithiacyclononane ([9]aneS$_3$), 1,4,7,10-tetrathiacyclododecane ([12]aneS$_4$), 1,5,9,13-tetrathiacyclohexadecane ([16]aneS$_4$) and 1,4,7,10,13,16-hexathiacyclooctadecane ([18]aneS$_6$). In contrast, the co-ordination chemistry of larger rings such as 1,4,7,10,13,16,19,22-octathiacyclotetracosane ([24]aneS$_8$) and 1,4,8,11,15,18,22,25-octathiacyclooctacosane ([28]aneS$_8$) is practically unknown. Furthermore, only a few examples of thioether macrocyclic complexes of Cd^{II}, Pb^{II}, Hg^{II} and Au^I have been reported[16–20] and it is only recently that the corresponding co-ordination chemistry of Ag^I has received any attention.[21–28] Nevertheless, macrocyclic polythioethers remain a useful starting point in the design of selective metal complexation agents for soft d^{10} metal ions.[16,20,22,29]

As a continuation of our studies on macrocyclic thioether complexes of second and third row transition metal ions we report herein the synthesis and the electrochemical properties of the complexes of Ag^I, Hg^{II} and Au^I with [24]aneS$_8$ and [28]aneS$_8$. In particular, the structures of the silver(I)[30] and mercury(II) complexes of [24]aneS$_8$ and the gold(I) and silver(I) complexes of [28]aneS$_8$ are described; these, together with $[Cu_2([24]aneS_8)][BF_4]_2$ and $[Cu_2([28]aneS_8)][ClO_4]_2$[3] represent the only complexes of these large-ring crown thioethers to be structurally characterised.[31]

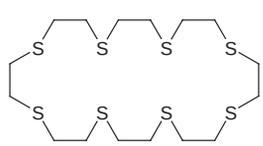

[24]aneS$_8$

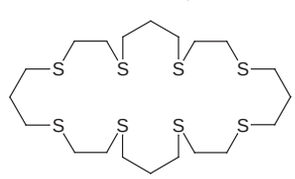

[28]aneS$_8$

Results and Discussion

$[(HgBr_2)_2([24]aneS_8)]$

Stirring [24]aneS$_8$ with 2 molar equivalents of $HgBr_2$ in CH_2Cl_2–MeCN (1:1 v/v ratio) for 12 h at room temperature affords a white precipitate. Analytical and mass spectrometric data for this product are consistent with the stoichiometry $(HgBr_2)_2$-[24]aneS$_8$. The analogous complex with [28]aneS$_8$ can be prepared in the same way as a white microcrystalline powder. However, colourless block-shaped crystals of adequate diffraction quality were only obtained for the complex with [24]aneS$_8$, by vapour diffusion of Et_2O into a solution of the complex in MeCN.

A single crystal structure analysis confirms the complex to be the binuclear species $[(HgBr_2)_2([24]aneS_8)]$ (Fig. 1). This

Table 1 Selected bond lengths (Å), angles and torsion angles (°) for $[(HgBr_2)_2([24]aneS_8)]$

Hg(1)–Br(1)	2.511(2)	Hg(1)–S(4)	2.835(4)
Hg(1)–Br(2)	2.588(2)	Hg(1)–S(7)	2.581(4)
Br(1)–Hg(1)–Br(2)	120.76(7)	Br(2)–Hg(1)–S(4)	84.87(9)
Br(1)–Hg(1)–S(4)	118.03(10)	Br(2)–Hg(1)–S(7)	110.77(10)
Br(1)–Hg(1)–S(7)	125.66(10)	S(4)–Hg(1)–S(7)	80.89(12)
$C(12^i)$–S(1)–C(2)–C(3)	−65.8(14)		
S(1)–C(2)–C(3)–S(4)	−53.8(15)		
C(2)–C(3)–S(4)–C(5)	−156.9(12)		
C(3)–S(4)–C(5)–C(6)	−62.4(15)		
S(4)–C(5)–C(6)–S(7)	−64(2)		
C(5)–C(6)–S(7)–C(8)	−79.2(15)		
C(6)–S(7)–C(8)–C(9)	−173.7(14)		
S(7)–C(8)–C(9)–S(10)	−61(2)		
C(8)–C(9)–S(10)–C(11)	126.3(14)		
C(9)–S(10)–C(11)–C(12)	−71(2)		
S(10)–C(11)–C(12)–$S(1^i)$	172.3(11)		
C(11)–C(12)–$S(1^i)$–$C(2^i)$	61.7(15)		

Symmetry transformation used to generate equivalent atoms: i $-x + 2$, $-y$, $-z$.

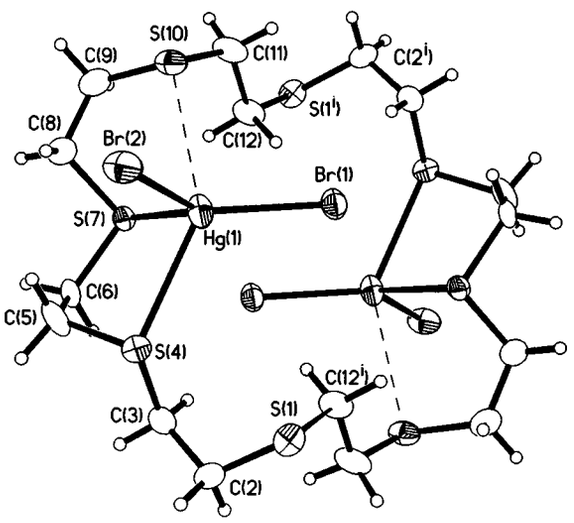

Fig. 1 View of $[(HgBr_2)_2([24]aneS_8)]$ with the numbering scheme adopted; i $-x + 2$, $-y$, $-z$. Displacement ellipsoids are drawn at 50% probability

molecule lies across a crystallographic inversion centre and the asymmetric unit therefore consists of one $HgBr_2$ moiety and half of a $[24]aneS_8$ macrocycle. Each Hg^{II} essentially has a distorted tetrahedral geometry, being co-ordinated to two consecutive S atoms of the macrocycle and to two Br^- ligands; Hg(1)–Br(1) 2.511(2), Hg(1)–Br(2) 2.588(2), Hg(1)–S(4) 2.835(4) and Hg(1)–S(7) 2.581(4) Å. Two factors can be suggested to explain the clear inequivalence of the Hg–S bond distances in this complex. One is the different dispositions of the two co-ordinated S-donors relative to the cavity of the macrocycle, S(4) being *endo*- and S(7) being *exo*-oriented; the other is the presence of a short interaction of 3.110(4) Å between the metal centre and the S(10) donor (Fig. 1). Including this interaction, the metal centres have an overall distorted trigonal bipyramidal geometry with the S(4) and S(10) donors occupying the apical positions [S(4)–Hg(1)–S(10) 146.3(13)°]. The Hg···Hg distance across the inversion centre is 5.476(2) Å with one $HgBr_2$ moiety situated above the mean plane of the macrocycle and the other positioned below to give an overall *anti* configuration. Moreover, the two bulky $HgBr_2$ groups are oriented towards the centre of the large macrocyclic cavity.

Selected molecular geometry parameters are summarised in Table 1. The crystal lattice comprises stacks of the binuclear

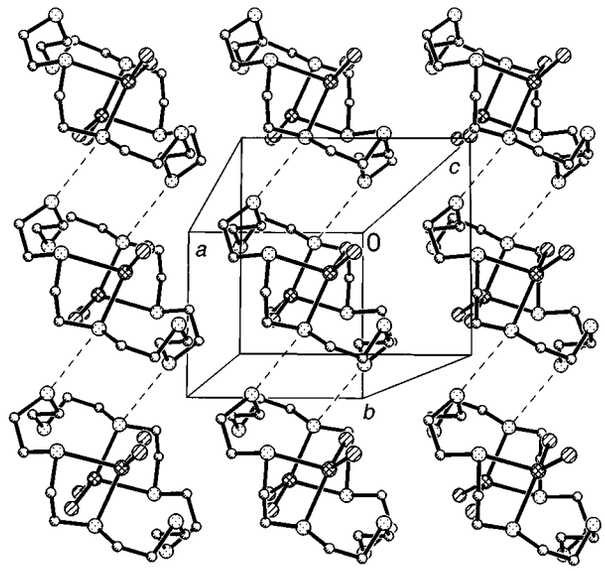

Fig. 2 Packing diagram for $[(HgBr_2)_2([24]aneS_8)]$ viewed along the *c* axis

complex which propagate along the crystallographic *b* axis *via* S···S contacts of 3.529(6) Å between successive units (Fig. 2). The structure of $[(HgBr_2)_2([24]aneS_8)]$ resembles that reported for $[(HgCl_2)_2([14]aneS_4)]$[17] and that proposed for $[(HgCl_2)_2([16]aneS_4)]$.[19] Halide ligands seem to have a marked effect on the co-ordination chemistry of Hg^{II} with macrocyclic polythioethers; they prevent occupation of all co-ordination sites by S-donors while still allowing a tetrahedral geometry at the metal centre. Interestingly, the structures of $[Hg([14]aneS_4)(OH_2)(ClO_4)_2]$,[17] $[Hg([15]aneS_5)(PF_6)_2]$,[18] $[Hg([16]aneS_4)(ClO_4)_2]$,[16b,19] and $[Hg([9]aneS_3)_2(PF_6)_2]$[16a] all show the metal ion in co-ordination geometries other than tetrahedral (either distorted square pyramidal or distorted octahedral) involving all the available sulfur atoms of the ligands. Further examples arise in the complexes $[\{(HgI_2)_2([14]aneS_4)\}_\infty]$[32] and $[\{(HgCl_2)_2([6]aneS_3)\}_\infty]$[33] in which the HgX_2 moieties bridge between two macrocycles acting as monodentate ligands.

Cyclic voltammetry of $[(HgBr_2)_2([24]aneS_8)]$ in dmf at 298 K (0.1 M $NBu^n_4PF_6$ supporting electrolyte) at platinum electrodes shows two irreversible reductions at $E_{pc} = -0.50$ and -0.80 V *vs.* ferrocene–ferrocenium at a scan rate of 100 mV s^{-1}. Controlled-potential electrolysis in dmf at 298 K confirms each of these processes to be two-electron transfers generating colourless solutions. The colourless solution obtained after reductive electrolysis by two electrons was EPR silent as a frozen glass, consistent with the formation of Hg^I–Hg^I or Hg^0–Hg^{II} species. Controlled-potential re-oxidation gives rise to a colourless solution having the same cyclic voltammogram as that of the starting material. The two irreversible reduction processes can therefore be assigned to formation of Hg^I–Hg^I or Hg^0–Hg^{II}, and Hg^0–Hg^0 species, respectively. Significantly, therefore, the two metal centres can be reduced by two electrons per Hg. For the overall four-electron process, metal deposition on the platinum electrode or in solution is not apparent visually, suggesting that Hg^0 might remain bound or associated with the thioether crown. The irreversibility of the reductive processes in the cyclic voltammogram is probably due either to a change in the co-ordination geometry of the reduced metal centres coupled with Hg^I–Hg^I interactions, or to separate, sequential two-electron reductions of each mercury centre separately. For mononuclear mercury(II) thioether complexes such as $[Hg([15]aneS_5)]^{2+}$ and $[Hg([18]aneN_2S_4)]^{2+}$ only one irreversible reductions are observed at +0.17 and −1.16 V *vs.* ferrocene–ferrocenium, respectively,[18] whereas one reversible reduction is observed for $[Hg([9]aneS_3)_2]^{2+}$ at −0.15 V.[16a]

The complex $[(HgBr_2)_2([28]aneS_8)]$ shows similar electro-

chemical behaviour to that of $[(HgBr_2)_2([24]aneS_8)]$. Cyclic voltammetry in dmf at 298 K (0.1 M $NBu^n_4PF_6$ supporting electrolyte) at platinum electrodes shows two irreversible reductions at $E_{pc} = -0.40$ and -0.70 V at a scan rate of 100 mV s^{-1}. Controlled-potential electrolysis in dmf at 298 K confirms each of these processes to be two-electron transfers to generate colourless solutions, with no metal deposition on the platinum electrode apparent. In this case also the solution obtained after the electrolysis at -0.55 V was EPR silent as a frozen glass indicating an Hg^I–Hg^I interaction in the resulting reduced complex or the formation of an Hg^0–Hg^{II} species.

Table 2 Selected bond lengths (Å), angles and torsion angles (°) for $[\{Ag_2([24]aneS_8)(CF_3SO_3)_2(MeCN)_2\}_\infty]$

Ag(1)–S(1)	2.5400(14)	Ag(1)–S(10^i)	2.5984(14)
Ag(1)–S(7^i)	2.556(2)	Ag(1)–S(4)	2.627(2)
S(1)–Ag(1)–S(7^i)	127.36(5)	S(1)–Ag(1)–S(4)	86.12(4)
S(1)–Ag(1)–S(10^i)	121.61(5)	S(7^i)–Ag(1)–S(4)	122.97(5)
S(7^i)–Ag(1)–S(10^i)	85.83(5)	S(10^i)–Ag(1)–S(4)	116.89(5)
C(12^{ii})–S(1)–C(2)–C(3)	68.8(4)		
S(1)–C(2)–C(3)–S(4)	64.2(5)		
C(2)–C(3)–S(4)–C(5)	73.2(5)		
C(3)–S(4)–C(5)–C(6)	169.9(4)		
S(4)–C(5)–C(6)–S(7)	−79.0(5)		
C(5)–C(6)–S(7)–C(8)	114.7(4)		
C(6)–S(7)–C(8)–C(9)	−76.9(5)		
S(7)–C(8)–C(9)–S(10)	−57.7(5)		
C(8)–C(9)–S(10)–C(11)	−68.8(4)		
C(9)–S(10)–C(11)–C(12)	−76.7(4)		
S(10)–C(11)–C(12)–S(1^{ii})	−71.7(5)		
C(11)–C(12)–S(1^{ii})–C(2^{ii})	119.7(4)		

Symmetry transformations used to generate equivalent atoms: i x, $y + 1$, z; ii $-x$, $-y$, $-z$.

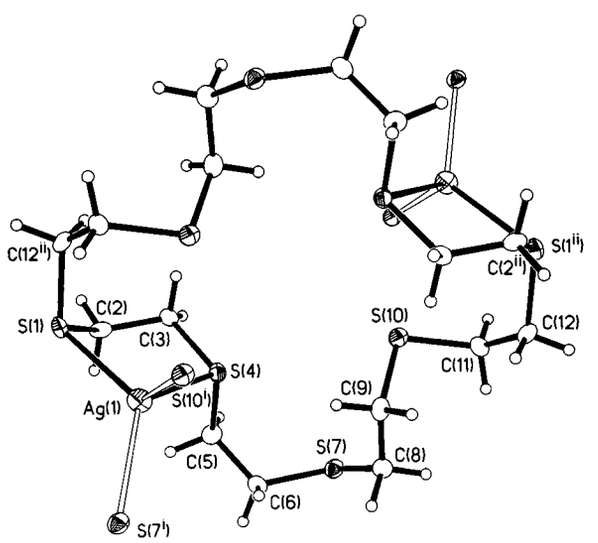

Fig. 3 View of the partial molecular structure of $[\{Ag_2([24]aneS_8)^{2+}\}_\infty]$ showing two asymmetric units and links to the polymeric structure (hollow bonds) with the numbering scheme adopted; i x, $y + 1$, z; ii $-x$, $-y$, $-z$. Displacement ellipsoids are drawn at the 50% probability level

$[\{Ag_2([24]aneS_8)(CF_3SO_3)_2(MeCN)_2\}_\infty]$ and $[Ag_2([28]aneS_8)][NO_3]_2$

Reaction of $[24]aneS_8$ with 2 molar equivalents of $Ag(O_3SCF_3)$ in CH_2Cl_2–MeCN (1:1 v/v ratio) affords a white precipitate after 1 h stirring at room temperature, for which microanalytical and mass spectrometric data support the stoichiometry $[Ag_2([24]aneS_8)(CF_3SO_3)_2(MeCN)_2]$. Colourless plates suitable for X-ray diffraction studies were obtained by vapour diffusion of Et_2O into a solution of the complex in MeCN. A single crystal structure determination of the complex[30] shows each Ag^I in a distorted tetrahedral environment co-ordinated to four S-donors, Ag–S 2.5400(14)–2.627(2) Å, S–Ag–S 85.83(5)–127.36(5)° (Fig. 3, Table 2) from two different ligand molecules; pairs of symmetry related silver(I) ions bridge pairs of macrocyclic ligands forming an infinite ladder running along the crystallographic b axis (Fig. 4) within which all eight S-donors of each $[24]aneS_8$ molecule are engaged in co-ordination to Ag^I. Each metal centre acts as the spiro-centre for two almost perpendicular AgS_2C_2 cyclic fragments (Fig. 4). The polymeric chains are separated by layers of $CF_3SO_3^-$ ions and MeCN molecules.

The formation of polymeric structures by d^{10} transition metal ion complexes of thioether crowns seems to be dependent on the tetrahedral environment of the metal centre. Thus, complexes such as $[\{(HgI_2)_2([14]aneS_4)\}_\infty]$,[32] $[\{Cu([14]aneS_4)(ClO_4)\}_\infty]$,[34] $[\{Ag([18]aneS_6)(Br)\}_\infty]$,[26] $[\{Ag([12]aneS_3)(CF_3SO_3)(MeCN)\}_\infty]$,[26] $[\{Ag\{(OH)_2[16]aneS_4\}(NO_3)\}_\infty]$[12] and $[\{Ag\{(OH)_2[16]aneS_4\}(O_2CMe)\}_\infty]$[12] all show the metal ions in tetrahedral environments linking two or more macrocyclic ligand molecules to form one- or three-dimensional polymeric networks. To confirm this idea, we argued that the larger 28-membered ring macrocycle $[28]aneS_8$ would have a sufficiently large cavity to encapsulate two silver(I) centres, making the possibility of a polymeric or bridged species less likely than in the smaller 24-membered ring analogue. Reaction of $[28]aneS_8$ with 2 molar equivalents of $AgNO_3$ in CH_2Cl_2–MeCN (1:1 v/v ratio) affords a colourless solution from which well shaped crystals of $[Ag_2([28]aneS_8)][NO_3]_2$ are obtained after partial removal of the solvent and diethyl ether diffusion. A single crystal structure determination shows the complex to be binuclear rather than polymeric, with two Ag^I placed within the cavity of $[28]aneS_8$ in a very distorted trigonal bipyramidal environment (Fig. 5). The three equatorial co-ordination sites and one of the axial positions are taken up by four S-donors from the macrocycle, Ag–S 2.4921(11)–2.8932(12) Å, S–Ag–S 80.30(3)–136.98(4)° (Table 3); the second axial position of the trigonal bipyramid is instead occupied by one oxygen atom O(2) from the NO_3^- counter anion, Ag(1)–O(2) 2.759(3) Å,

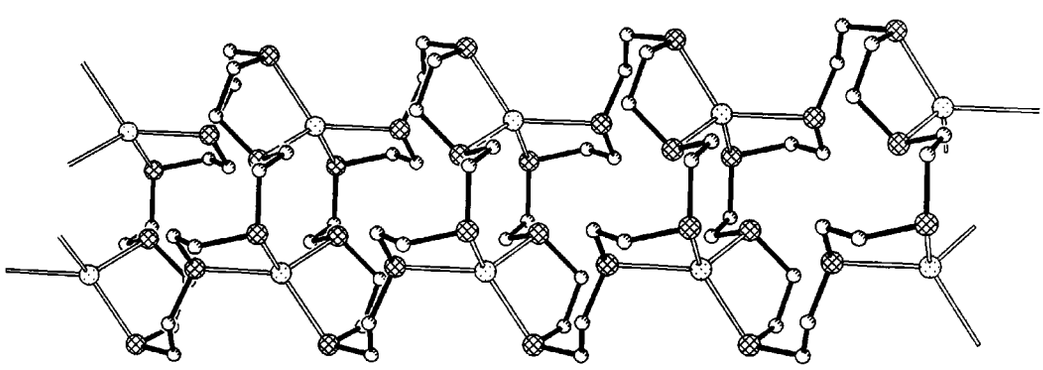

Fig. 4 Packing diagram for the $[\{Ag_2([24]aneS_8)^{2+}\}_\infty]$ polymeric chain viewed along the c axis

Table 3 Selected bond lengths (Å), angles and torsion angles (°) for $[Ag_2([28]aneS_8)][NO_3]_2$

Ag(1)–S(1)	2.5257(12)	Ag(1)–S(11)	2.4921(11)
Ag(1)–S(4)	2.6314(11)	Ag(1)–O(2)	2.759(3)
Ag(1)–S(8)	2.8932(12)		
S(1)–Ag(1)–S(4)	86.33(4)	S(8)–Ag(1)–S(11)	80.30(3)
S(1)–Ag(1)–S(8)	114.85(4)	O(2)–Ag(1)–S(1)	91.71(8)
S(1)–Ag(1)–S(11)	136.98(4)	O(2)–Ag(1)–S(4)	78.77(8)
S(4)–Ag(1)–S(8)	86.16(3)	O(2)–Ag(1)–S(8)	148.57(8)
S(4)–Ag(1)–S(11)	136.26(4)	O(2)–Ag(1)–S(11)	91.72(8)
$C(14^i)$–S(1)–C(2)–C(3)	66.7(3)		
S(1)–C(2)–C(3)–S(4)	60.5(4)		
C(2)–C(3)–S(4)–C(5)	64.8(3)		
C(3)–S(4)–C(5)–C(6)	177.2(3)		
S(4)–C(5)–C(6)–C(7)	56.2(5)		
C(5)–C(6)–C(7)–S(8)	50.3(5)		
C(6)–C(7)–S(8)–C(9)	173.7(3)		
C(7)–S(8)–C(9)–C(10)	126.5(3)		
S(8)–C(9)–C(10)–S(11)	−70.0(4)		
C(9)–C(10)–S(11)–C(12)	173.0(3)		
C(10)–S(11)–C(12)–C(13)	70.2(3)		
S(11)–C(12)–C(13)–C(14)	−173.9(3)		
C(12)–C(13)–C(14)–$S(1^i)$	−66.9(4)		
C(13)–C(14)–$S(1^i)$–$C(2^i)$	−147.8(3)		

Symmetry transformation used to generate equivalent atoms: i $-x$, $-y+1$, $-z+2$.

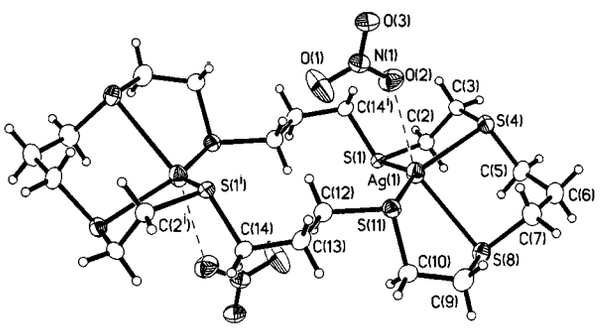

Fig. 5 View of $[Ag_2([28]aneS_8)][NO_3]_2$ with the numbering scheme adopted; i $-x$, $-y+1$, $-z+2$. Displacement ellipsoids are drawn at 50% probability

O(2)–Ag(1)–S(8) 148.57(8)°. The crystal lattice features chains of the binuclear complex which propagate along the crystallographic *a* axis *via* S···S contacts of 3.327(2) Å between successive units (Fig. 6).

Cyclic voltammetry of $[\{Ag_2([24]aneS_8)(CF_3SO_3)_2(MeCN)_2\}_\infty]$ measured in dmf at 298 K (0.1 M $NBu^n_4PF_6$ supporting electrolyte) at platinum electrodes shows two irreversible reductions at $E_{pc} = -0.38$ and -0.64 V and an intense desorption spike at 0 V at a scan rate of 100 mV s^{-1}. The first reduction occurs at similar redox potentials to the Ag^I–Ag^0 couples in $[Ag([15]aneS_5)]^+$ and $[Ag([18]aneS_6)]^+$ observed at -0.37 and -0.42 V respectively,[35a] whereas the second correspond to the reduction potentials observed for the couple Ag^I–Ag^0 in $[Ag([18]aneN_2S_4)]^+$, $[Ag(Me_2[18]aneN_2S_4)]^+$ and $[Ag([9]aneS_3)_2]^+$ which range from -0.57 to -0.78 V.[35a] Controlled potential reductions in dmf at 298 K confirm each of the reduction processes to be single-electron transfers giving rise to colourless solutions and a black layer of Ag^0 on the platinum electrode. In this case therefore the two metal centres are not reduced simultaneously at the same potential. Furthermore, as a consequence of the reduction of Ag^I to Ag^0 demetallation of the complex is observed. No oxidation waves are observed in the cyclic voltammogram up to +2.0 V. Nevertheless, if the complex is treated with concentrated (98%) H_2SO_4 a transient purple species is formed. The X-band EPR spectrum measured as a frozen glass at 77 K shows a weak rhombic signal with

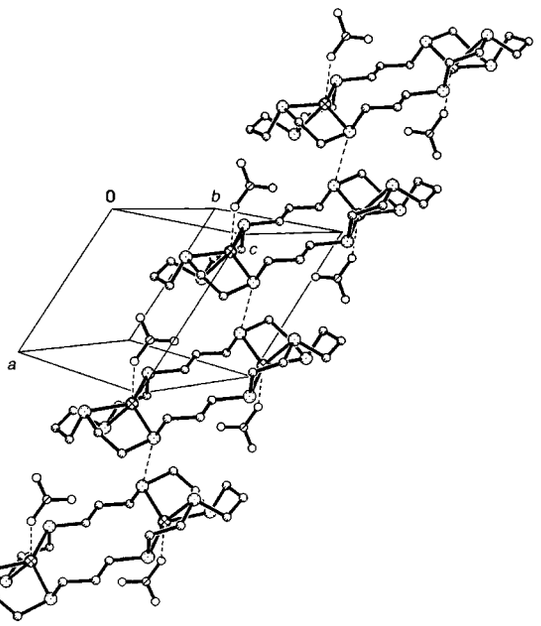

Fig. 6 Packing diagram for $[Ag_2([28]aneS_8)][NO_3]_2$

$g_1 = 2.0392$, $g_2 = 2.0174$, $g_3 = 1.9911$ with hyperfine coupling to ^{107}Ag and ^{109}Ag not being observed. The use of acidic media for oxidation of complexes of thioether crowns is based upon the stabilisation of the products *via* inhibition of base-promoted ring opening reactions.[35b]

The cyclic voltammetry of $[Ag_2([28]aneS_8)][NO_3]_2$ measured in dmf at 298 K (0.1 M $NBu^n_4PF_6$ supporting electrolyte) is very similar to that recorded for $[\{Ag_2([24]aneS_8)(CF_3SO_3)_2(MeCN)_2\}_\infty]$. Two irreversible reductions are observed at $E_{pc} = -0.10$ and -0.50 V together with an intense desorption spike at 0 V at a scan rate of 100 mV s^{-1}. In this case also, controlled coulometric measurements in dmf confirm the two reductions to be single-electron processes giving rise to colourless solutions and a black layer of Ag^0 on the platinum electrode. The complex can be oxidised chemically with 98% H_2SO_4 to give a transient purple species which shows a weak rhombic signal in the EPR spectrum measured as a frozen glass at 77 K with $g_1 = 2.0388$, $g_2 = 2.0243$, $g_3 = 1.9905$. As before, hyperfine coupling to ^{107}Ag and ^{109}Ag is not observed in the X-band. Significantly, on chemical oxidation, silver(I) complexes of [12]aneS$_4$, [14]aneS$_4$, [16]aneS$_4$, [15]aneS$_5$ and [18]aneS$_6$ all give more stable purple-blue silver(II) species with comparable EPR spectral parameters, where hyperfine coupling to ^{107}Ag and ^{109}Ag is observable in Q-band EPR spectra.[35a]

$[Au_2([28]aneS_8)][PF_6]_2$ and $[Au_2([24]aneS_8)][PF_6]_2$

Reaction of [28]aneS$_8$ with 2 molar equivalents of $[Au(tht)_2]PF_6$ (tht = tetrahydrothiophene) in $MeNO_2$ affords a white precipitate upon addition of ice-cold Et_2O. The product shows FAB mass spectral peaks (M^+) at *m/z* 1075, 929 and 733 assigned to $[^{197}Au_2([28]aneS_8)(PF_6)]^+$, $[^{197}Au_2([28]aneS_8 - H)]^+$ and $[^{197}Au([28]aneS_8)]^+$ respectively. On the basis of this evidence together with microanalytical and IR spectroscopic data the product is assigned as $[Au_2([28]aneS_8)][PF_6]_2$. A single crystal structure determination confirmed the compound to be a genuine binuclear gold(I) complex (Fig. 7, Table 4). The two encapsulated gold(I) centres are related by a crystallographic inversion centre and are each co-ordinated to two S-donors, Au–S(1) 2.330(2) Au–S(11) 2.338(2) Å, with two additional longer interactions, Au–S(4) 2.789(2), Au–S(8) 2.763(2) Å conferring a [2 + 2] distorted tetrahedral geometry on the metal ion. The co-ordination at Au^I is comparable to that observed for Cu^I in the analogous $[Cu_2([28]aneS_8)]^{2+}$ cation,[3] the main difference being the angle at S(1)–M–S(11). The preference of Au^I for linear co-

Table 4 Selected bond lengths (Å), angles and torsion angles (°) for $[Au_2([28]aneS_8)][PF_6]_2$

Au(1)–S(1)	2.330(2)	Au(1)–S(8)	2.763(2)
Au(1)–S(4)	2.789(2)	Au(1)–S(11)	2.338(2)
S(1)–Au(1)–S(4)	86.24(6)	S(4)–Au(1)–S(8)	91.88(6)
S(1)–Au(1)–S(8)	108.14(6)	S(4)–Au(1)–S(11)	113.93(6)
S(1)–Au(1)–S(11)	155.58(6)	S(8)–Au(1)–S(11)	87.77(6)
S(1)–C(2)–C(3)–S(4)	60.1(7)		
C(2)–C(3)–S(4)–C(5)	77.8(6)		
C(3)–S(4)–C(5)–C(6)	−95.1(6)		
S(4)–C(5)–C(6)–C(7)	−63.5(8)		
C(5)–C(6)–C(7)–S(8)	114.3(6)		
C(6)–C(7)–S(8)–C(9)	−167.8(5)		
C(7)–S(8)–C(9)–C(10)	67.9(6)		
S(8)–C(9)–C(10)–S(11)	57.2(7)		
C(9)–C(10)–S(11)–C(12)	63.3(6)		
C(10)–S(11)–C(12)–C(13)	65.8(6)		
S(11)–C(12)–C(13)–C(14)	166.7(5)		
C(12)–C(13)–C(14)–S(1^i)	−71.2(7)		
C(13)–C(14)–S(1^i)–C(2^i)	−157.3(5)		
C(14)–S(1^i)–C(2^i)–C(3^i)	−73.8(6)		

Symmetry transformation used to generate equivalent atoms: i $2-x$, $-y$, $-z$.

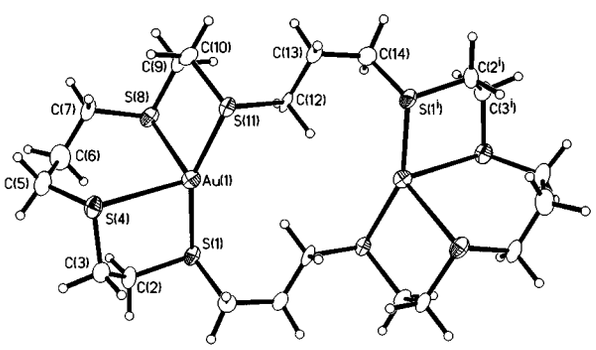

Fig. 7 View of $[Au_2([28]aneS_8)]^{2+}$ with the numbering scheme adopted; i $-x+2$, $-y$, $-z$. Displacement ellipsoids are drawn at 50% probability

ordination with thioether donors is reflected in the opening up of this angle to 155.58(6) from 133.4(2)° in the copper(I) cation. The greater distortion of the tetrahedral geometry for the gold(I) complex pulls the gold(I) centres closer together, to 5.6977(6) Å in comparison to 6.454(3) Å between the two Cu^I centres. Interestingly, the [2 + 2] distorted tetrahedral stereochemistry at Au^I in $[Au_2([28]aneS_8)][PF_6]_2$ is very similar to that observed for Au^I when bound to other thioether ligands, *e.g.* [9]$aneS_3$, [18]$aneS_6$ and [15]$aneS_5$.[35a]

Cyclic voltammetry of $[Au_2([28]aneS_8)][PF_6]_2$ at platinum electrodes in MeCN at 298 K (0.1 M $NBu^n_4PF_6$) shows a broad chemically reversible oxidation at $E_{\frac{1}{2}} = +0.55$ V ($\Delta E_p = 230$ mV) at a scan rate of 140 mV s^{-1}. Coulometric measurements confirmed this process to be a four-electron transfer step. Electrochemical oxidation of $[Au_2([28]aneS_8)][PF_6]_2$ at +1.0 V affords a pale yellow, EPR silent species, consistent with the production of a binuclear gold(III) species. During the oxidation of the colourless gold(I) complex to the pale yellow gold(III) product transient, paramagnetic canary yellow species are formed. The EPR spectrum recorded for the intermediate species as a frozen glass at 77 K shows a complicated multiplet ($g_{av} \approx 2.019$). The return reduction to $[Au_2([28]aneS_8)]^{2+}$ involves the same intermediate(s). The oxidation of $[Au_2([28]aneS_8)]^{2+}$ to $[Au_2([28]aneS_8)]^{6+}$ therefore involves EPR active gold(II) intermediates, with signals arising from mixtures of the intermediate species Au^I–Au^{II}, Au^{II}–Au^{II} and Au^{II}–Au^{III}. The Au^{II}–Au^{II} species may be EPR silent in the presence of metal–metal interactions.

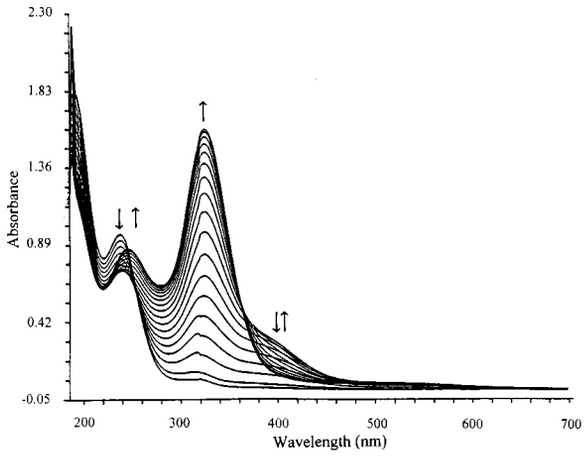

Fig. 8 *In situ* electronic spectrum for conversion of $[Au_2([28]aneS_8)]^{2+}$ into $[Au_2([28]aneS_8)]^{6+}$ (OTE, MeCN, 0.1 M $NBu^n_4PF_6$, 253 K, +1.0 V *vs.* ferrocene–ferrocenium)

The four-electron oxidation of $[Au_2([28]aneS_8)][PF_6]_2$ was also monitored by UV/VIS spectroscopy. The *in situ* electrochemical oxidation of $[Au_2([28]aneS_8)][PF_6]_2$ was carried out in MeCN (0.1 M $NBu^n_4PF_6$) at 253 K (Fig. 8). The study shows the conversion of $[Au_2([28]aneS_8)]^{2+}$ [$\lambda_{max} = 238$ nm ($\varepsilon_{max} = 17\,500$ M^{-1} cm^{-1})] to $[Au_2([28]aneS_8)]^{6+}$ [$\lambda_{max} = 324$ ($\varepsilon_{max} = 26\,750$) and 245 nm (14 770 M^{-1} cm^{-1})] at +1.0 V. The oxidation proceeds through an intermediate species, confirmed by the presence of the overlapping band at $\lambda_{max} = 400$ nm. This process is chemically reversible with the starting material being regenerated on re-reduction at +0.1 V. We have reported previously the stabilisation of mononuclear gold(II) centres by thioether crowns.[15] In general, this has been achieved *via* control of the ligation environment to afford elongated octahedral co-ordination at the d^9 metal centre. In the absence of additional ligands, gold(II) centres within the complex cation $[Au_2([28]aneS_8)]^{x+}$ would be expected to retain four-co-ordination and would therefore be readily oxidised to d^8 Au^{III} for which four-co-ordinate, square-planar co-ordination is preferred. It appears therefore that [28]$aneS_8$ is capable of supporting the four-electron oxidation of distorted tetrahedral Au^I_2 to square-planar Au^{III}_2 within its own co-ordination sphere.

The reaction of [24]$aneS_8$ with 2 molar equivalents of $[Au(tht)_2]PF_6$ in $MeNO_2$ affords a white precipitate on the addition of Et_2O for which analytical and mass spectroscopic data support the stoichiometry $[Au_2([24]aneS_8)][PF_6]_2$. Unfortunately the complex proved to be unstable both in solution and in the solid state, making further characterisation difficult. Attempts to grow suitable single crystals for a crystal structure determination resulted in decomposition of the complex to colloidal gold. Owing to this instability, a pure sample of $[Au_2([24]aneS_8)][PF_6]_2$ for electrochemical studies was not obtained. These results suggest that the gold(I) centres are bound in very strained stereochemistries by [24]$aneS_8$ in comparison to the unstrained co-ordination at Au^I in the stable [28]$aneS_8$ analogue. This is a function of the smaller ring size of [24]$aneS_8$ in comparison to [28]$aneS_8$ which may promote demetallation of the binuclear complex to form a mononuclear species.

Experimental

Melting points are uncorrected. The IR spectra were recorded as KBr discs using a Perkin-Elmer 598 spectrometer over the range 200–4000 cm^{-1}. Microanalyses were performed by the University of Nottingham Chemistry Department Microanalytical service. Electrochemical measurements were performed on a Bruker E310 Universal Modular Polarograph. All readings were taken using a three-electrode potentiostatic

Table 5 Crystallographic data

	$[(HgBr_2)_2([24]aneS_8)]$	$[Ag_2([24]aneS_8)(CF_3SO_3)_2(MeCN)_2]$	$[Au_2([28]aneS_8)][PF_6]_2$	$[Ag_2([28]aneS_8)][NO_3]_2$
Formula	$C_{16}H_{32}Br_4Hg_2S_8$	$C_{22}H_{38}Ag_2F_6N_2O_6S_{10}$	$C_{20}H_{40}Au_2F_{12}P_2S_8$	$C_{20}H_{40}Ag_2N_2O_6S_8$
M	1201.72	1076.88	1220.76	876.76
Crystal system	Monoclinic	Monoclinic	Monoclinic	Triclinic
Space group	$P2_1/n$ (no. 14)	$P2_1/c$ (no. 14)	$P2_1/n$ (no. 14)	$P\bar{1}$ (no. 2)
a/Å	8.5311(11)	13.285(2)	6.6156(14)	8.9759(14)
b/Å	8.100(4)	6.3340(10)	19.836(5)	9.584(2)
c/Å	22.425(3)	22.547(3)	13.190(6)	11.200(2)
α/°				109.83(2)
β/°	100.461(14)	94.752(9)	97.73(2)	94.43(2)
γ/°				116.95(2)
U/Å^3	1523.9(8)	1890.7(5)	1715	776.7(2)
Z	2	2	2	1
T/K	150(2)	150(2)	173(1)	150(2)
μ(Mo-Kα)/mm^{-1}	15.862	1.656	9.171	1.837
Reflections collected	3112	3344	3166	2765
Unique reflections, R_{int}	2877, 0.088	3344, —	2166, 0.0156	2734, 0.0347
T_{min}, T_{max}	0.016, 0.059	0.61, 0.81	0.074, 0.188	0.494, 0.657
$R1$	0.0626 [2190 $F \geqslant 4\sigma(F)$]	0.0431 [2255 $F \geqslant 4\sigma(F)$]	—	0.0326[2493 $F \geqslant 4\sigma(F)$]
$wR2$ (all data)[37,38]	0.1766	0.0779	—	0.0709
R[39]	—	—	0.0288 [1912 $F \geqslant 6\sigma(F)$]	—
R'[39]	—	—	0.0336	—

system in dmf and/or MeCN containing 0.1 M $NBu^n_4PF_6$ as supporting electrolyte. Cyclic voltammetric measurements were carried out using a double platinum electrode and an Ag–AgCl reference electrode. The UV/VIS spectra were measured in quartz cells using a Perkin-Elmer Lambda 9 spectrophotometer, mass spectra at the EPSRC National Mass Spectrometry Service at Swansea and EPR spectra on Bruker EMX 6/1 and Bruker ER-200D spectrometers. The complex $[Au(tht)_2]PF_6$ was prepared as reported in the literature.[36]

Preparations

$[(HgBr_2)_2([24]aneS_8)]$. To a well stirred solution of $[24]aneS_8$ (25 mg, 0.052 mmol) in CH_2Cl_2–MeCN (20 cm^3, 1:1 v/v ratio) was added a solution of $HgBr_2$ (37.5 g, 0.104 mmol) in MeCN (5 cm^3). The mixture was stirred at room temperature overnight, and the resulting white precipitate was filtered off, washed with CH_2Cl_2 and dried *in vacuo* (38.4 mg, 61.5% yield). Colourless blocks suitable for X-ray diffraction studies were grown by diffusion of diethyl ether vapour into a MeCN solution of the white solid. M.p. 130 °C [Found (Calc. for $C_8H_{16}Br_2HgS_4$): C, 16.04 (15.99); H, 2.72 (2.68%)]. IR spectrum (KBr disc): 2955w, 2911m, 1411s, 1250s, 1211m, 1144m, 905m, 861w and 822w cm^{-1}. ES$^+$ mass spectrum: m/z = 1204; calc. for $[(^{202}HgBr_2)_2([24]aneS_8)]^+$ (M^+) 1204, with the correct isotopic distribution.

$[(HgBr_2)_2([28]aneS_8)]$. A solution of $HgBr_2$ (67.04 mg, 0.186 mmol) in MeCN (6 cm^3) was added to a well stirred solution of $[28]aneS_8$ (50 mg, 0.093 mmol) in CH_2Cl_2 (10 cm^3). After 10 min stirring a white solid started precipitating. The mixture was stirred for 3 h at room temperature, and the resulting white precipitate filtered off, washed with CH_2Cl_2 and dried *in vacuo* (64 mg, 76.6% yield). M.p. 168–170 °C [Found (Calc. for $C_{10}H_{20}Br_2HgS_4$): C, 18.87 (19.10); H, 2.95 (3.21%)]. FAB mass spectrum (3-nitrobenzyl alcohol matrix): very poor ionisation and the expected ions were not found. IR spectrum (KBr disc): 2917m, 1439m, 1405s, 1344w, 1255m, 889w, 844w, 722w, 683w and 628w cm^{-1}.

$[\{Ag_2([24]aneS_8)(CF_3SO_3)_2(MeCN)_2\}_\infty]$. To a well stirred solution of $[24]aneS_8$ (50 mg, 0.104 mmol) in CH_2Cl_2–MeCN (20 cm^3, 1:1 v/v ratio) was added a solution of $Ag(O_3SCF_3)$ (53.44 mg, 0.208 mmol) in MeCN (5 cm^3). The mixture was stirred at room temperature for 1 h. The white solid was filtered off and dried *in vacuo* (70 mg, 62.5% yield). Colourless blocks suitable for X-ray diffraction studies were grown by diffusion of diethyl ether vapour into a MeCN solution of the white solid. M.p. 182–184 °C [Found (Calc. for $C_{11}H_{19}AgF_3NO_3S_5$): C, 21.85 (21.74); H, 3.35 (3.21); N, 2.45 (2.60%)]. IR spectrum (KBr disc): 2967w, 2900w, 2255w, 1427m, 1405m, 1278vs, 1255vs, 1155s, 1027s, 905w, 822w, 755w, 633s, 572w and 511m cm^{-1}. FAB mass spectrum (3-nitrobenzyl alcohol matrix): m/z = 845, 695 and 589; calc. for $[^{107}Ag_2([24]aneS_8)(CF_3SO_3)]^+$ (M^+) 845, $[^{107}Ag_2([24]aneS_8)]^+$ (M^+) 695 and $[^{107}Ag([24]aneS_8)]^+$ (M^+) 589, with the correct isotopic distributions.

$[Ag_2([28]aneS_8)][NO_3]_2$. Reaction of $[28]aneS_8$ (19.9 mg, 0.037 mmol) with $AgNO_3$ (12.57 mg, 0.074 mmol) in stirring CH_2Cl_2–MeCN (1:1 v/v, 10 cm^3) for 2 h in the dark gave a colourless solution, which was then reduced in volume (2.5 cm^3) under reduced pressure. Crystallisation by Et_2O diffusion afforded colourless irregular plates (27.1 mg, 83.54% yield). M.p. 180 °C with decomposition [Found (Calc. for $C_{10}H_{20}AgNO_3S_4$): C, 27.35 (27.40); H, 4.62 (4.60); N, 3.24 (3.19%)]. IR spectrum (KBr disc): 2918w, 1646w, 1439s, 1370s, 1250s, 1150m, 901m, 824m, 748w and 725w cm^{-1}. FAB mass spectrum (3-nitrobenzyl alcohol matrix): m/z = 814, 751 and 645; calc. for $[^{107}Ag_2([28]aneS_8)(NO_3)]^+$ (M^+) 813, $[^{107}Ag_2([24]aneS_8)]^+$ (M^+) 751 and $[^{107}Ag([24]aneS_8)]^+$ (M^+) 644, with correct isotopic distributions.

$[Au_2([24]aneS_8)][PF_6]_2$. Reaction of $[24]aneS_8$ (40 mg, 0.083 mmol) with $[Au(tht)_2]PF_6$ (90 mg, 0.174 mmol) in stirring $MeNO_2$ (10 cm^3) for 3 h in the dark gave a colourless solution, which was then reduced in volume (5 cm^3) *in vacuo*. Filtration into ice-cold Et_2O (30 cm^3) afforded a white precipitate on cooling to −20 °C (72 mg, 28% yield) [Found (Calc. for $C_8H_{16}AuF_6PS_4$): C, 17.8 (16.5); H, 3.01 (2.75%)]. IR spectrum (KBr disc): 2960w, 2920w, 1420m, 1260m, 1200m, 1140m, 860–840s and 560m cm^{-1}. FAB mass spectrum (3-nitrobenzyl alcohol matrix): m/z = 1019, 873 and 677; calc. for $[^{197}Au_2([24]aneS_8)(PF_6)]^+$ (M^+) 1019, $[^{197}Au_2([24]aneS_8 - H)]^+$ (M^+) 873 and $[^{197}Au([24]aneS_8)]^+$ (M^+) 677, with correct isotopic distributions.

$[Au_2([28]aneS_8)][PF_6]_2$. Reaction of $[28]aneS_8$ (40 mg, 0.075 mmol) with $[Au(tht)_2]PF_6$ (83 mg, 0.160 mmol) in stirring $MeNO_2$ (10 cm^3) for 3 h in the dark gave a colourless solution, which was then reduced in volume (3 cm^3) *in vacuo*. Filtration into ice-cold Et_2O (30 cm^3) afforded a white precipitate on cooling to −20 °C. The product was filtered off and washed with Et_2O and CH_2Cl_2, yielding a white microcrystalline solid which was dried *in vacuo* and stored at −20 °C (yield 82 mg, 75%)

[Found (Calc. for $C_{10}H_{20}AuF_6PS_4$): C, 19.7 (19.7); H, 3.26 (3.30%)]. IR spectrum (KBr disc): 2910w, 2860w, 1550m, 1440m, 1420m, 1340w, 1300w, 1260m, 1250m, 1240m, 1200m, 1140m, 1040s, 920m, 860m, 840w, 740w, 650w and 555w cm^{-1}. FAB mass spectrum (3-nitrobenzyl alcohol matrix): m/z = 1075, 929 and 733; calc. for $[^{197}Au_2([28]aneS_8)(PF_6)]^+$ (M^+) 1075, $[^{197}Au_2([28]aneS_8 - H)]^+$ (M^+) 929 and $[^{197}Au([28]aneS_8)]^+$ (M^+) 733, with correct isotopic distributions.

X-Ray crystallography

A summary of the crystal data and refinement details for $[(HgBr_2)_2([24]aneS_8)]$, $[\{Ag_2([24]aneS_8)(CF_3SO_3)_2(MeCN)_2\}_\infty]$, $[Au_2([28]aneS_8)][PF_6]_2$ and $[Ag_2([28]aneS_8)][NO_3]_2$ is given in Table 5. The crystals were cooled using an Oxford Cryosystems open-flow nitrogen cryostat[40] and data were collected using a Stoe Stadi-4 four-circle diffractometer using ω–θ scans. Data were corrected for Lorentz-polarisation effects and absorption corrections were applied by using ψ scans; for $[Au_2([28]aneS_8)][PF_6]_2$, corrections for absorption were applied at isotropic convergence using DIFABS.[41] The structures were solved by direct methods[42] and subsequent Fourier-difference syntheses;[37,38] for $[Au_2([28]aneS_8)][PF_6]_2$ the structure was solved by Patterson synthesis and subsequent refinement by least squares on F.[39] All non-H atoms were refined anisotropically and all H atoms placed at calculated positions (CH_2) or located from a circular ΔF synthesis (CH_3) and thereafter refined with $U_{iso}(H) = xU_{eq}(C)$ (x = 1.2 for CH_2, 1.5 for CH_3). For the mercury complex the largest residual electron density features lay near the Hg and Br atoms.

CCDC reference number 186/1058.

See http://www.rsc.org/suppdata/dt/1998/2931/ for crystallographic files in .cif format.

Acknowledgements

We thank the EPSRC, The University of Nottingham and the EPSRC National Mass Spectrometry Service at Swansea for support.

References

1 S. R. Cooper, *Acc. Chem. Res.*, 1988, **21**, 141; A. J. Blake and M. Schröder, *Adv. Inorg. Chem.*, 1990, **35**, 1; S. C. Rawle and S. R. Cooper, *Struct. Bonding* (*Berlin*), 1991, **72**, 1.
2 T. Adachi, M. D. Durrant, D. L. Hughes, C. J. Pickett, R. L. Richards, J. Talarmin and T. Yoshiba, *J. Chem. Soc.*, *Chem. Commun.*, 1992, 1464.
3 A. J. Blake, A. Taylor and M. Schröder, *Polyhedron*, 1990, **9**, 2911.
4 A. J. Blake, R. O. Gould, A. J. Holder, A. J. Lavery and M. Schröder, *Polyhedron*, 1990, **9**, 2919.
5 A. J. Blake, M. A. Halcrow and M. Schröder, *J. Chem. Soc.*, *Dalton Trans.*, 1994, 1631 and refs. therein.
6 C. Landgrafe and W. S. Sheldrick, *J. Chem. Soc.*, *Dalton Trans.*, 1996, 989.
7 K. Brandt and W. S. Sheldrick, *J. Chem. Soc.*, *Dalton Trans.*, 1996, 1237.
8 A. J. Blake, D. W. Bruce, I. A. Fallis, S. Parsons, H. Richtzenhain, S. A. Ross and M. Schröder, *Philos. Trans. R. Soc. London*, *Ser. A*, 1996, **354**, 395.
9 R. D. Adams, S. B. Fallon, J. L. Perrin, J. A. Queisser and J. H. Yamamoto, *Chem. Ber.*, 1996, **129**, 313 and refs. therein.
10 G. J. Grant, K. E. Rogers, W. N. Setzer and D. G. Van Derveer, *Inorg. Chim. Acta*, 1995, **234**, 35.
11 H.-J. Kim, J.-H. Lee, I.-H. Suh and Y. Do, *Inorg. Chem.*, 1995, **34**, 796.
12 M. Munakata, L. P. Wu, M. Yamamoto, T. Kuroda-Sowa and M. Maekawa, *J. Chem. Soc.*, *Dalton Trans.*, 1995, 3215.
13 G. R. Willey, A. Jarvis, J. Palin and W. Errington, *J. Chem. Soc.*, *Dalton Trans.*, 1994, 255; A. J. Blake, G. Reid and M. Schröder, *J. Chem. Soc.*, *Dalton Trans.*, 1992, 2987; G. R. Willey, M. T. Lakin and N. W. Alcock, *J. Chem. Soc.*, *Dalton Trans.*, 1992, 591; A. J. Blake, R. O. Gould, C. Radek and M. Schröder, *J. Chem. Soc.*, *Chem. Commun.*, 1993, 1191.
14 A. J. Blake, A. J. Holder, T. J. Hyde and M. Schröder, *J. Chem. Soc.*, *Chem. Commun.*, 1987, 987; A. J. Blake, R. O. Gould, A. J. Holder, T. I. Hyde, A. J. Lavery, M. O. Odulate and M. Schröder, *J. Chem. Soc.*, *Chem. Commun.*, 1987, 118; S. C. Rawle, R. Yagbasan and S. R. Cooper, *J. Am. Chem. Soc.*, 1987, **109**, 6181; A. J. Blake, R. O. Gould, A. J. Holder, T. I. Hyde and M. Schröder, *J. Chem. Soc.*, *Dalton Trans.*, 1988, 1861.
15 A. J. Blake, R. O. Gould, J. A. Greig, A. J. Holder, T. I. Hyde and M. Schröder, *J. Chem. Soc.*, *Chem. Commun.*, 1989, 876; A. J. Blake, R. O. Gould, J. A. Greig, A. J. Holder, T. I. Hyde, A. Taylor and M. Schröder, *Angew. Chem.*, 1990, **102**, 203; *Angew. Chem.*, *Int. Ed. Engl.*, 1990, **29**, 197; A. J. Blake, A. Taylor and M. Schröder, *J. Chem. Soc.*, *Chem. Commun.*, 1993, 1097.
16 (*a*) A. J. Blake, A. J. Holder, T. I. Hyde, G. Reid and M. Schröder, *Polyhedron*, 1989, **8**, 2041; (*b*) W. N. Setzer, Q. Guo, G. J. Grant, J. L. Hubbard, R. L. Glass and D. G. VanDerveer, *Heteroatom Chem.*, 1990, **1**, 317; (*c*) T. E. Jones, L. S. W. L. Sokol, D. B. Rorabacker and M. D. Glick, *J. Chem. Soc.*, *Chem. Commun.*, 1979, 140.
17 N. Alcock, N. Herron and P. Moore, *J. Chem. Soc.*, *Dalton Trans.*, 1978, 394.
18 A. J. Blake, E. C. Pasteur, G. Reid and M. Schröder, *Polyhedron*, 1991, **10**, 1545.
19 W. N. Setzer, Y. Tang, G. J. Grant and D. G. VanDerveer, *Inorg. Chem.*, 1991, **30**, 3652.
20 W. N. Setzer, Y. Tang, G. J. Grant and D. G. VanDerveer, *Inorg. Chem.*, 1992, **31**, 1116.
21 A. J. Blake, R. O. Gould, G. Reid and M. Schröder, *J. Chem. Soc.*, *Chem. Commun.*, 1990, 974.
22 B. De Groot and S. J. Loeb, *Inorg. Chem.*, 1991, **30**, 3103.
23 A. J. Blake, R. O. Gould, A. J. Holder, T. I. Hyde and M. Schröder, *Polyhedron*, 1989, **8**, 513.
24 H. J. Küppers, K. Wieghardt, Y. H. Tsay, C. Krüger, B. Nuber and J. Weiss, *Angew. Chem.*, *Int. Ed. Engl.*, 1987, **26**, 575.
25 J. Clarkson, R. Yagbasan, P. J. Blower, S. C. Rawle and S. R. Cooper, *J. Chem. Soc.*, *Chem. Commun.*, 1987, 950.
26 P. J. Blower, J. A. Clarkson, S. C. Rawle, J. R. Hartman, R. E. Wolf, jun., R. Yagbsan, S. G. Bott and S. R. Cooper, *Inorg. Chem.*, 1989, **28**, 4040.
27 A. J. Blake, D. Collison, R. O. Gould, G. Reid and M. Schröder, *J. Chem. Soc.*, *Dalton Trans.*, 1993, 521.
28 R. Alberto, W. Nef, A. Smith, T. A. Kaden, M. Neuburger, M. Zehnder, A. Frey, U. Abram and P. A. Schubiger, *Inorg. Chem.*, 1996, **35**, 3420.
29 G. Wu, W. Jiang, J. D. Lamb, J. S. Bradshaw and R. M. Izatt, *J. Am. Chem. Soc.*, 1991, **113**, 6538.
30 A. J. Blake, W.-S. Li, V. Lippolis and M. Schröder, *Chem. Commun.*, 1997, 1943.
31 R. E. Desimone and T. M. Tighe, *J. Inorg. Nucl. Chem.*, 1976, **38**, 1623; K. Travis and D. H. Busch, *Chem. Commun.*, 1970, 1041; A. C. Braithwaite, C. E. F. Rickard and T. N. Waters, *Aust. J. Chem.*, 1981, **34**, 2665; K. Saito, Y. Masudo and E. Sekido, *Anal. Chim. Acta*, 1983, **151**, 447; D. Sedvic and H. Meider, *J. Inorg. Nucl. Chem.*, 1977, **39**, 1403.
32 N. Galesic, M. Herceg and D. Sevdic, *Acta Crystallogr.*, *Sect. C*, 1986, **42**, 565.
33 W. R. Costello, A. T. McPhail and G. A. Sim, *J. Chem. Soc. A*, 1966, 1190.
34 E. R. Dockal, L. L. Diaddario, M. D. Glick and D. B. Rorabacher, *J. Am. Chem. Soc.*, 1977, **99**, 4530.
35 (*a*) A. J. Blake, D. Collison, R. O. Gould, A. J. Holder, T. I. Hyde, G. Reid, A. Taylor and M. Schröder, in *Molecular Electrochemistry of Inorganic, Bioinorganic and Organometallic Compounds*, eds. A. J. L. Pombiero and J. A. McCleverty, 1993, p. 121; (*b*) A. J. Blake, A. J. Holder, T. I. Hyde, H.-J. Küppers, M. Schröder, S. Stötzel and K. Wieghardt, *J. Chem. Soc.*, *Chem. Commun.*, 1989, 1600.
36 R. Usòn, A. Laguna, A. Navarro, R. V. Parish and L. S. Moore, *Inorg. Chim. Acta*, 1986, **112**, 205.
37 G. M. Sheldrick, SHELXL 93, University of Göttingen, 1993.
38 G. M. Sheldrick, SHELXL 97, University of Göttingen, 1997.
39 G. M. Sheldrick, SHELX 76, University of Cambridge, 1976.
40 J. Cosier and A. M. Glazer, *J. Appl. Crystallogr.*, 1986, **19**, 105.
41 N. Walker and D. Stuart, DIFABS, Program for Empirical Absorption Corrections, *Acta Crystallogr.*, *Sect. A*, 1983, **39**, 158.
42 G. M. Sheldrick, SHELXS 86, *Acta Crystallogr.*, *Sect. A*, 1990, **46**, 467.

Received 5*th May* 1998; *Paper* 8/03358G